ARL-TR-7829 ● SEP 2016

US Army Research Laboratory

Thermal Fluid Analysis of the Heat Sink and Chip Carrier Assembly for a US Army Research Laboratory Liquid-Fueled Thermophotovoltaic Power Source Demonstrator

by William R Allmon and C Mike Waits

NOTICES

Disclaimers

The findings in this report are not to be construed as an official Department of the Army position unless so designated by other authorized documents.

Citation of manufacturer's or trade names does not constitute an official endorsement or approval of the use thereof.

Destroy this report when it is no longer needed. Do not return it to the originator.

ARL-TR-7829 ● SEP 2016

US Army Research Laboratory

Thermal Fluid Analysis of the Heat Sink and Chip Carrier Assembly for a US Army Research Laboratory Liquid-Fueled Thermophotovoltaic Power Source Demonstrator

by William R Allmon and C Mike Waits
Sensors and Electron Devices Directorate, ARL

REPORT DOCUMENTATION PAGE

Form Approved
OMB No. 0704-0188

1. REPORT DATE *(DD-MM-YYYY)*	2. REPORT TYPE	3. DATES COVERED (From - To)
September 2016	Technical Report	06/2016

4. TITLE AND SUBTITLE
Thermal Fluid Analysis of the Heat Sink and Chip Carrier Assembly for a US Army Research Laboratory Liquid-Fueled Thermophotovoltaic Power Source Demonstrator

5a. CONTRACT NUMBER

5b. GRANT NUMBER

5c. PROGRAM ELEMENT NUMBER

6. AUTHOR(S)
William R Allmon and C Mike Waits

5d. PROJECT NUMBER

5e. TASK NUMBER

5f. WORK UNIT NUMBER

7. PERFORMING ORGANIZATION NAME(S) AND ADDRESS(ES)
US Army Research Laboratory
ATTN: RDRL-SED-E
2800 Powder Mill Road
Adelphi, MD 20783-1138

8. PERFORMING ORGANIZATION REPORT NUMBER
ARL-TR-7829

9. SPONSORING/MONITORING AGENCY NAME(S) AND ADDRESS(ES)

10. SPONSOR/MONITOR'S ACRONYM(S)

11. SPONSOR/MONITOR'S REPORT NUMBER(S)

12. DISTRIBUTION/AVAILABILITY STATEMENT
Approved for public release; distribution is unlimited.

13. SUPPLEMENTARY NOTES

14. ABSTRACT

Compact power sources with high energy and power densities are critical for many military applications. These applications span from personal or squad-level power sources for long-duration missions without resupply to unmanned air vehicles requiring only a few hours of running time. In the 10–100 W+ power range, battery technology is the best solution currently available, but higher-energy dense technologies are needed to augment batteries and extend the available energy density well beyond state-of-the-art battery technology. One way to approach this is to take advantage of the large energy content of hydrocarbons or alcohols. Conversion efficiencies of only a few percent can provide comparable energy density to battery technology with the added advantage of instant recharge. One technology being pursued by the US Army Research Laboratory is combustion-based thermophotovoltaic power sources. Combustion can be used to convert fuel to heat a surface to temperatures above 500 °C. To support this work, this report details the analysis of the chip carrier and water-cooled heat sink to control the temperature of the photovoltaic cell while exposed to radiation from the emitter.

15. SUBJECT TERMS
TPV, thermophotovoltaic, heat sink, power source, high energy density, fuel conversion

16. SECURITY CLASSIFICATION OF:			17. LIMITATION OF ABSTRACT	18. NUMBER OF PAGES	19a. NAME OF RESPONSIBLE PERSON
a. REPORT	b. ABSTRACT	c. THIS PAGE			William R Allmon
Unclassified	Unclassified	Unclassified	UU	32	19b. TELEPHONE NUMBER (Include area code) 301-394-0117

Contents

List of Figures

List of Tables

1. Introduction/Background

Compact power sources with high energy and power densities are critical for many military applications. These applications span from personal or squad-level power sources for long-duration missions without resupply to unmanned air vehicles requiring only a few hours of running time. In the 10–100 W+ power range, battery technology is the best solution currently available. But higher energy dense technologies are needed to augment batteries and extend the available energy density well beyond state-of-the-art battery technology (140 W·h/kg for rechargeable lithium-ion technology).[1]

One way to achieve higher energy density is to take advantage of the large energy content of hydrocarbons or alcohols. Conversion efficiencies of only a few percent can provide increased energy density compared to battery technology with the added advantage of instant recharge. One technology being pursued by the US Army Research Laboratory (ARL) is combustion-based thermophotovoltaic (TPV) power sources including a heat-recirculating microcombustor. Combustion can be used to convert fuel to heat a surface to temperatures above 500 °C.[1]

Figure 1 describes the primary components of a TPV system: a heat source, an emitter, and a photovoltaic converter. The heat source supplies thermal energy to the emitter, which radiates the energy across a gap to the photovoltaic cell or an array of photovoltaic cells. The photovoltaic cell(s) then converts the thermal radiation to electrical energy, which can be delivered to a load or conditioning circuitry. Optical filters between the emitter and the photovoltaic cell (not included in Fig. 1), as well as reflectors deposited on the backside of the photovoltaic cell, are also common components. The optical cavity between the emitter and photovoltaic cell is often held under vacuum to minimize conduction and convective heat transfer.[1] For the concept demonstrator being developed at ARL, the exterior of the microcombustor with the emitter mounted and photovoltaic cells will also be held at vacuum to minimize heat and radiation loss.

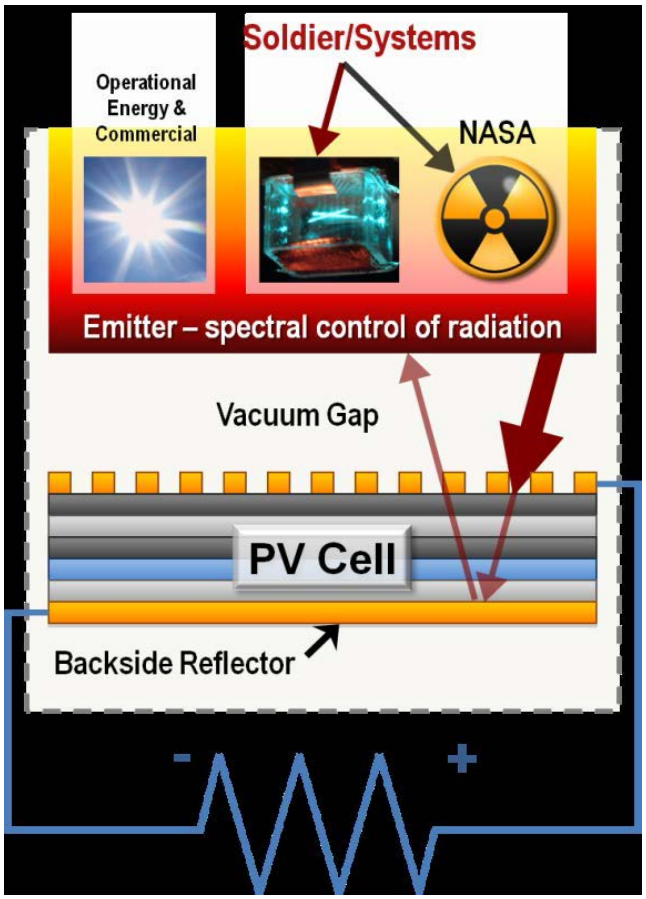

Fig. 1 Primary components of the TPV energy converter[1]

2. Objective

To support the development of the concept demonstrator, a chip carrier with a water-cooled heat sink is needed to control the temperature of the photovoltaic cells while exposed to the radiation from the emitter. The heat sink and chip carrier must control the temperature of the photovoltaic cells to at least as low as room temperature (25 °C). Controlling the temperature of the photovoltaic cells will allow for a parametric study of the effect of temperature on the photovoltaic cell performance and can therefore lead to minimizing cell thermal management requirements. Figure 2 shows the photovoltaic cells attached to the chip carrier, which is mounted to the heat sink with screws. The figure also shows the cooling water tubes, vacuum flange, and feedthroughs (electrical and thermocouple). The cooling water is supplied by a chiller (not shown). This report reports the analysis of the heat sink and chip carrier to control the temperature of the photovoltaic cell while exposed to radiation from the emitter.

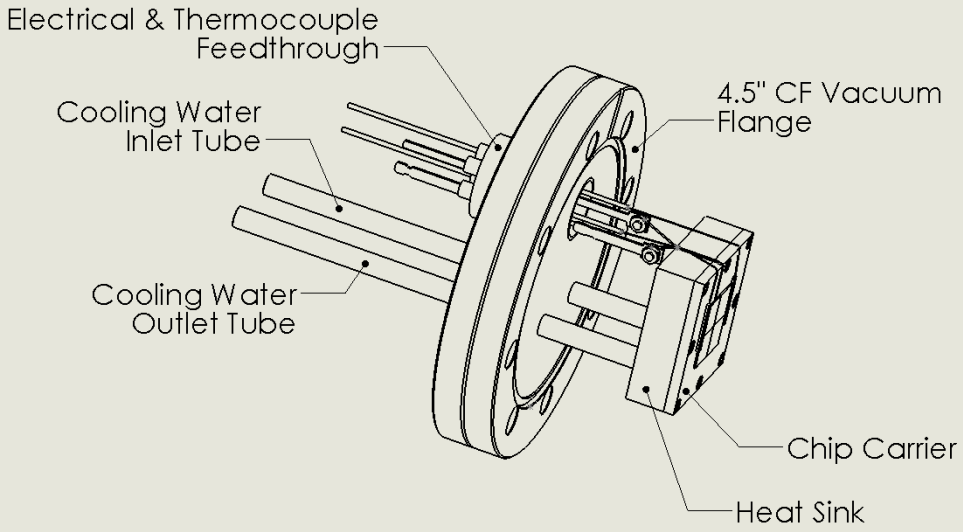

Fig. 2 Heat sink and chip carrier

Figure 3 shows the dimensions of the heat sink and chip carrier.

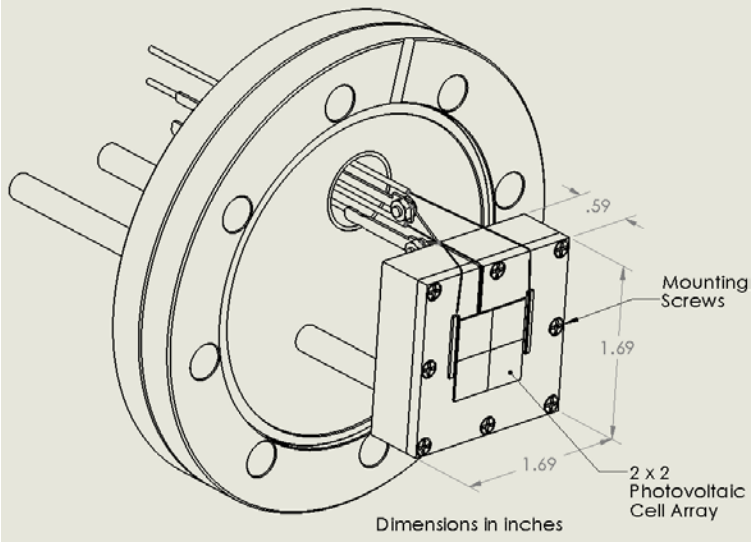

Fig. 3 Heat sink and chip carrier dimensions

Figure 4 shows the serpentine path for the water flowing through the heat sink.

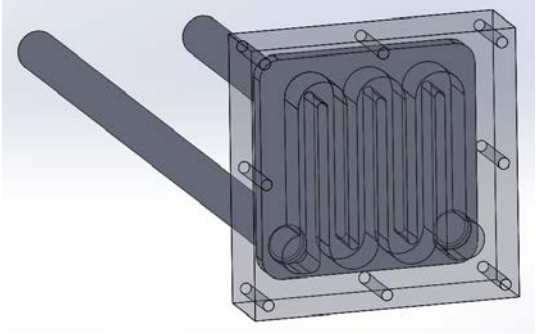

Fig. 4 Serpentine water flow path inside the heat sink

3. Simulation

Thermal fluid analysis enables analysis of conjugate heat transfer (thermal conduction in solids, convection between fluids and solids, and radiation) using computational fluid dynamics to detect hot spots, reduce overheating challenges, improve thermal isolation, and leverage thermal performance. This analysis was completed using Solid Works Flow Simulation, which can calculate either the steady-state or transient temperature fields due to heat transfer in solids (conduction); free, forced, and mixed convection; radiation; and heat sources (heat generation rate, heat power, and temperature).[2]

The geometry was simplified (Fig. 5) to make it easier to mesh and eliminate discontinuities in the mesh. Under General Settings, the internal analysis type was selected and cavities without flow conditions were excluded. Heat conduction in solids is included. Figure 6 shows the initial conditions in the General Settings.

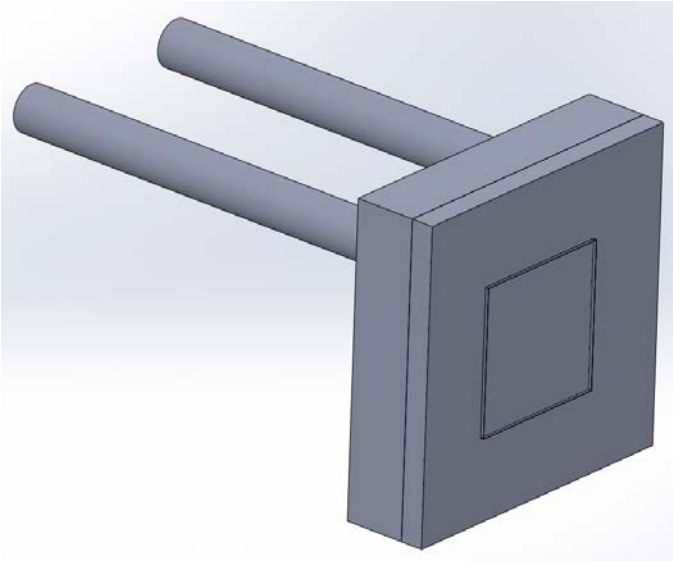

Fig. 5 Simplified geometry of the heat sink, chip carrier, and photovoltaic cell

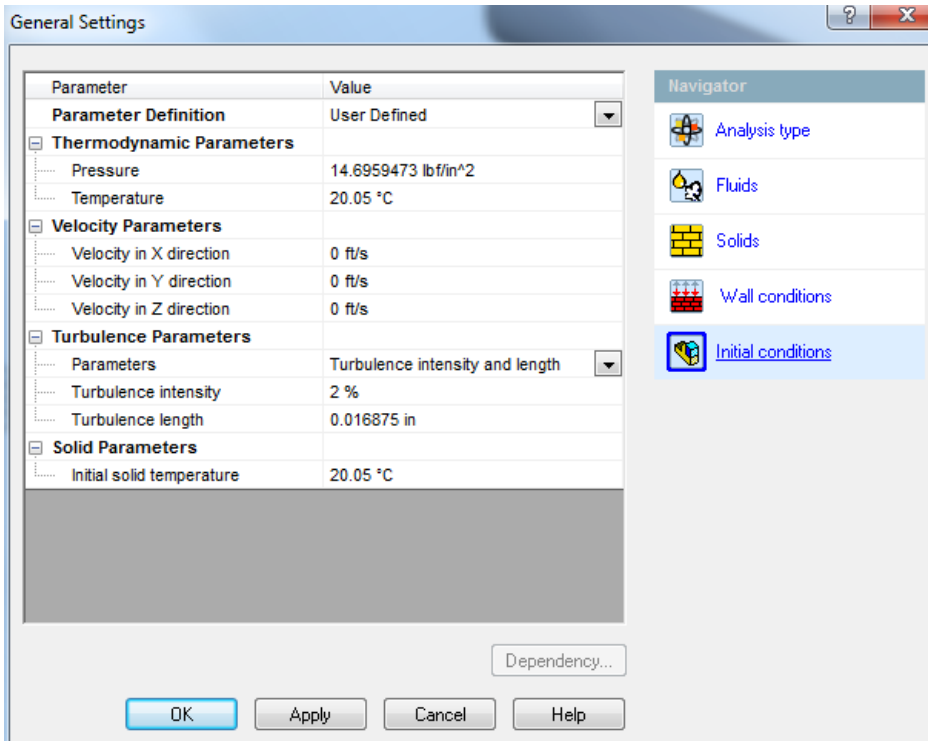

Fig. 6 Initial conditions in the General Settings

Heat conduction in solids as well as free and forced convection are included in the analysis. Radiation is applied as a heat generation rate to a surface based on the method described later in this section. The whole assembly is in vacuum so all outer surfaces are considered adiabatic. The conduction of heat through the tubes to the 4.5-inch CF vacuum flange shown in Fig. 2 is neglected, resulting in a more conservative estimate of the photovoltaic cell temperature.

For solids, such as the heat sink and tubes highlighted in blue in Fig. 7, a user-defined solid for 316 L stainless steel was added to the engineering database with the properties shown in Table 1.

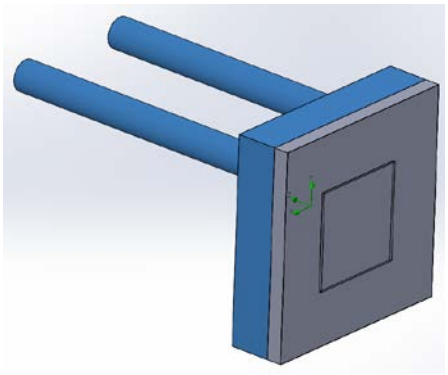

Fig. 7 Heat sink and tubes shown in blue

Table 1 Material properties used in the analysis

Material	Property	Temperature (K)	Value	Units
316 stainless steel	Density	…	8238	kg/m^3
	Specific heat	300	468	J/(kg*K)
		400	504	
		600	550	
		800	576	
		1000	602	
	Thermal conductivity	300	13.4	W/(m*K)
		400	15.2	
		600	18.3	
		800	21.3	
		1000	24.2	
Indium phosphide	Density	…	4810	kg/m^3
	Specific heat	298	309.8	J/(kg*K)
		323	312.3	
		373	317.3	
	Thermal conductivity	…	68	W/(m*K)
	Melting temperature	…	1333	K
Copper	Density	…	8960	kg/m^3
	Specific heat	8	0.4729	J/(kg*K)
		10	0.8709	
		15	2.907	
		20	7.29	
		40	58.76	
		80	202.6	
		150	322.6	
		250	373.3	
		298.1	384	
		400	397.5	
		600	416.7	
		1000	451.1	
		1356.2	475	
	Thermal conductivity	4	16200	W/(m*K)
		10	24000	
		20	10800	
		40	2170	
		80	560	
		150	429	
		200	413	

Table 1 Material properties used in the analysis (continued)

Material	Property	Temperature (K)	Value	Units
Copper	Thermal conductivity	300	401	W/(m*K)
		400	393	
		600	379	
		800	366	
		1000	352	
		1356.2	327	
	Melting temperature	…	1356.2	K

For the photovoltaic cell highlighted in blue in Fig. 8, a user-defined solid for indium phosphide was added to the engineering database with the properties shown in Table 1.

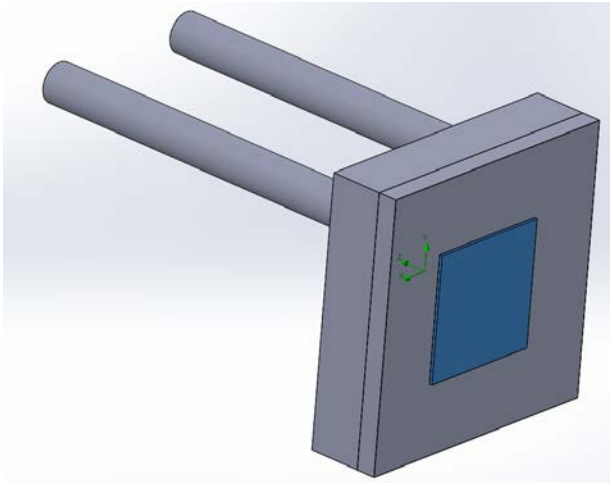

Fig. 8 Photovoltaic cell highlighted in blue

For the chip carrier highlighted in blue in Fig. 9, a user-defined solid for 316 L stainless steel was added to the engineering database or the existing properties in the engineering database for copper, both shown Table 1, were used.

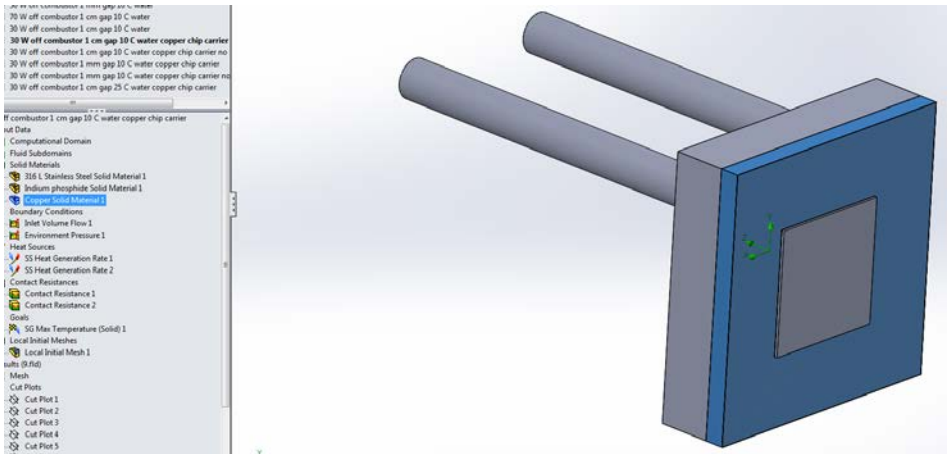

Fig. 9 Chip carrier highlighted in blue

For the cooling water, the existing properties in the engineering database were used. The inlet cooling water flow rate was set to 1.3 gpm (0.13368 ft^3/min) to match the Lytron Model RC006G03BB2 chiller and an outlet condition of 14.69 psig was applied to the outlet tube. The flow conditions were considered as laminar and turbulent.

Accurately modeling the thermal contact resistance between the chip carrier and the heat sink and the chip carrier and the photovoltaic cell is a big concern. For the interface between the chip carrier and heat sink, a thermal contact resistance of 6×10^{-4} m^2K/W for the stainless steel interfaces, under vacuum conditions and a contact pressure of 14.5 psi, was used throughout the analysis.[3] The chip carrier and the photovoltaic cell were attached using EPO-Tek H20E silver epoxy. According to the data sheet, for a TO-18 package with nickel-gold metalized 20 × 20-mil chips bonded with 2-mil-thick EPO-Tek H20E, the thermal resistance (junction to case) ranged from 6.7 to 7.0 K/W. Since thermal contact resistance (m^2 K/W) = R" = RA, letting R = 6.7 K/W and A = $(0.02 \text{ inch})^2 = (0.000508 \text{ m})^2$, R" = 1.72×10^{-6} m^2 K/W. This value was used throughout the analysis.

Radiation is applied as heat generated on the surfaces by calculating the incident radiation from the microcombustor surface emitting the radiation and considering the view factor between the chip carrier and the microcombustor and between the photovoltaic cell and microcombustor. Assuming a 1.69- × 1.69-inch chip carrier, a 2- × 2-cm photovoltaic cell, a 2- × 2-cm emitter, and a 1-cm distance between the emitter and the photovoltaic cell, it was calculated that 82% of the radiation is incident on both surfaces and 41% is incident on the photovoltaic cell.[4] Therefore, the remaining 41% of the radiation is incident on the surface of the chip carrier not covered by the photovoltaic cell. The difference in distance from the chip carrier to the microcombustor versus the photovoltaic cell to the microcombustor is

neglected. Assuming an emissivity of 0.9 and average T^4 temperatures of the surface, the Stefan Boltzmann equation says the emitter on one side of the microcombustor emits 70 W worse case, thus the heat generation rate of 70 W × 0.41 = 28.7 W was applied to the photovoltaic cell outer surface and the chip carrier surface not covered by the photovoltaic cell. As a more likely case, the microcombustor will emit 30 W. In this case, the heat generation rate of 30 W × 0.41 = 12.3 W was applied to the photovoltaic cell outer surface and the chip carrier surface not covered by the photovoltaic cell. Note 15% to 20% of the energy incident upon the photovoltaic cells will be converted to electricity. An additional case was run where no heat was applied to the chip carrier surface not covered by the photovoltaic cell.

For a 1-mm distance of between the photovoltaic cell and the emitter, it was calculated that 99.8% of the radiation is incident on both surfaces 90.8% is incident on the photovoltaic cell; therefore, 9% is incident on the area of the chip carrier around the photovoltaic cell. As discussed previously, a 70-W emission off one side of the combustor is the worst case, thus a heat generation rate of 70 W × 0.908 = 63.56 W was applied to the photovoltaic cell outer surface and 70 W × 0.09 = 6.3 W of was applied to the chip carrier surface not covered by the photovoltaic cell. For the more likely case of 30 W, as discussed previously, a heat generation rate of 30 W × 0.908 = 27.24 W was applied to the photovoltaic cell outer surface and 30 W × 0.09 = 2.7 W was applied to the chip carrier surface not covered by the photovoltaic cell.

4. Mesh

The mesh was set to level 3 with the minimum gap size manually set to 0.01 inch. A local mesh was applied to the face of the photovoltaic cell. The resulting mesh is shown in Fig. 10 with a close up view shown in Fig. 11. Figure 11 shows the mesh has a minimum of 4 cells through the thickness of critical components where a temperature gradient is expected such as the photovoltaic cell, chip carrier, heat sink walls, and the fluid.

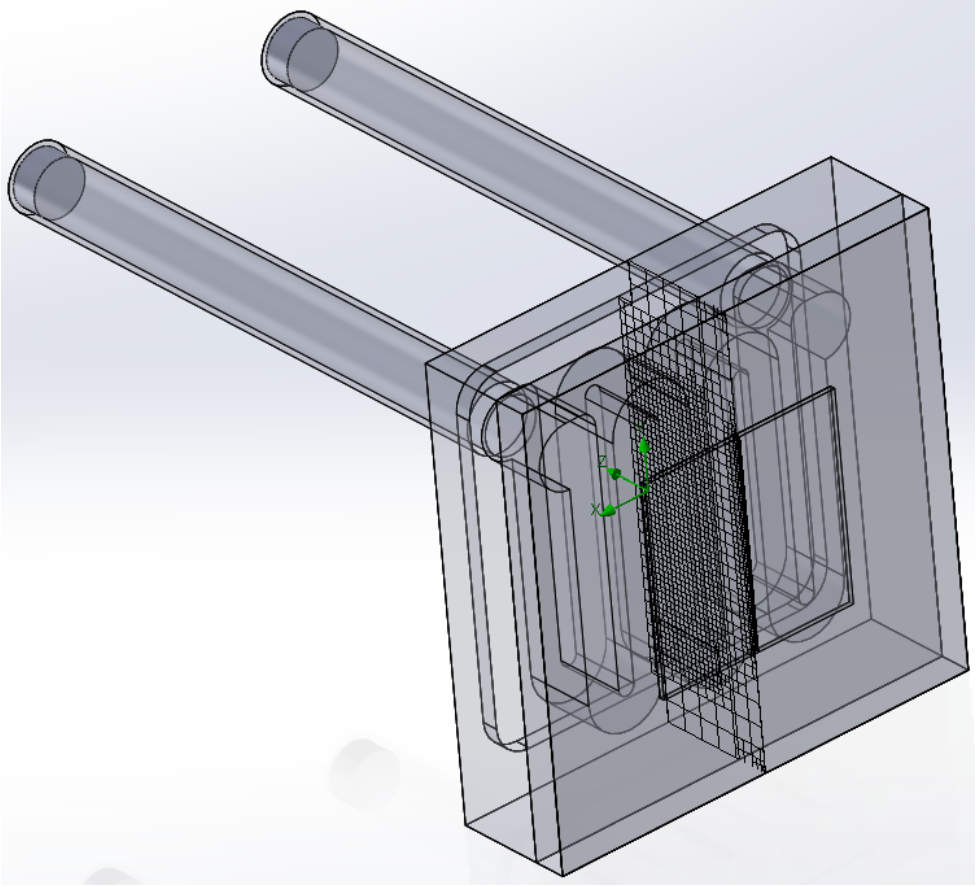

Fig. 10 Mesh

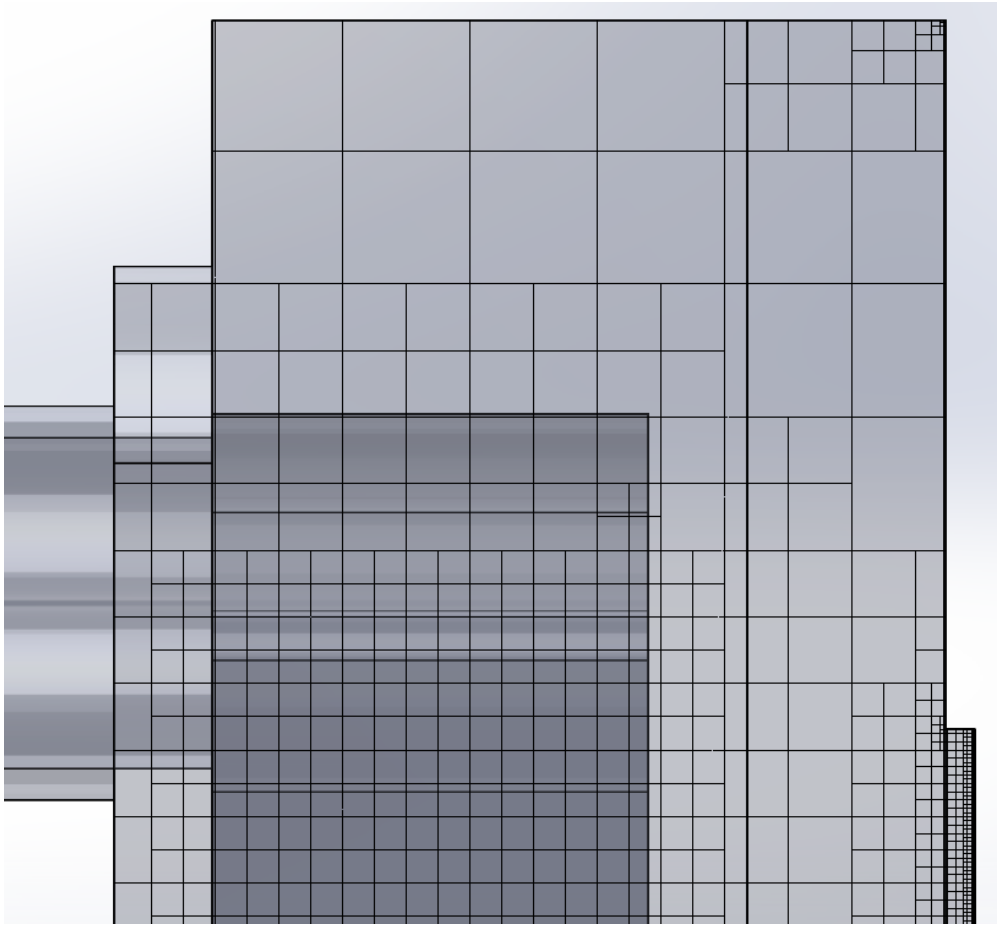

Fig. 11 Close-up view of the mesh

5. Results

Figures 12 through 16 show the results of cases where the distance from the emitter to the chip carrier was 1 cm and the power from the emitter was 30 W. This results in the application of 12.3 W to the surface of the photovoltaic cell and 12.3 W to the surface of the chip carrier not covered by the photovoltaic cell, with the exception of Case D, which has no power applied to the surface of the chip carrier not covered by the photovoltaic cell. The cooling water temperature was set to 20 or 10 °C. The chip carrier material was set to either 316 stainless steel or copper. Note the temperature scale varies from case to case thus for example areas of red in Case A are not the same temperature as areas of red in Case B.

Case	A	B	C	D
Distance:	1 cm	1 cm	1 cm	1cm
Heat generation rate:	30 W	30 W	30 W	30 W
-To Photovoltaic Cell:	12.3 W	12.3 W	12.3 W	12.3 W
-To Chip Carrier:	12.3 W	12.3 W	12.3 W	0 W
H2O Temp:	20 C	10 C	10 C	10 C
Chip Carrier Material:	316 Stainless Steel	316 Stainless Steel	Copper	Copper

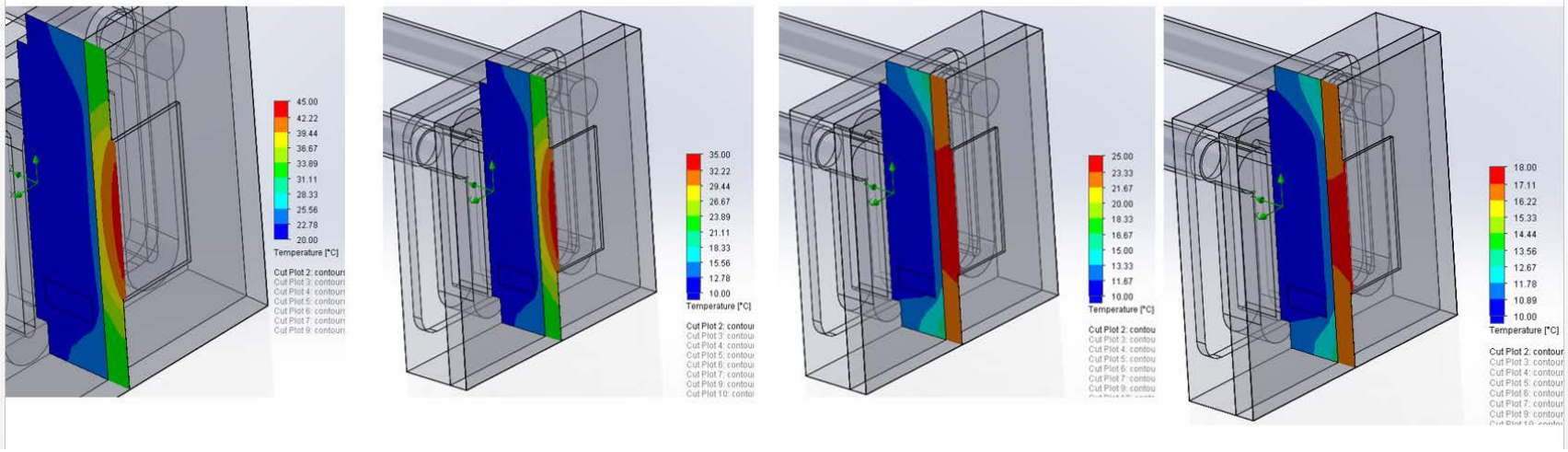

Fig. 12 Temperature profile for a cross section through the center of the assembly

Case	A	B	C	D
Distance:	1 cm	1 cm	1 cm	1cm
Heat generation rate:	30 W	30 W	30 W	30 W
- To Photovoltaic Cell:	12.3 W	12.3 W	12.3 W	12.3 W
- To Chip Carrier:	12.3 W	12.3 W	12.3 W	0 W
H2O Temp:	20 C	10 C	10 C	10 C
Chip Carrier Material:	316 Stainless Steel	316 Stainless Steel	Copper	Copper

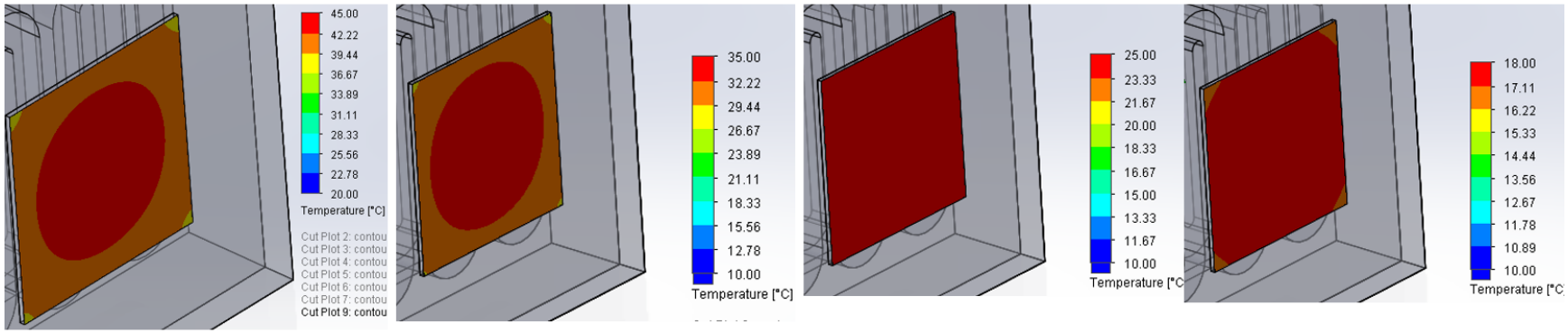

Fig. 13 Temperature distribution on the outer surface of the photovoltaic cell

Case	A	B	C	D
Distance:	1 cm	1 cm	1 cm	1cm
Heat generation rate:	30 W	30 W	30 W	30 W
- To Photovoltaic Cell:	12.3 W	12.3 W	12.3 W	12.3 W
- To Chip Carrier:	12.3 W	12.3 W	12.3 W	0 W
H2O Temp:	20 C	10 C	10 C	10 C
Chip Carrier Material:	316 Stainless Steel	316 Stainless Steel	Copper	Copper

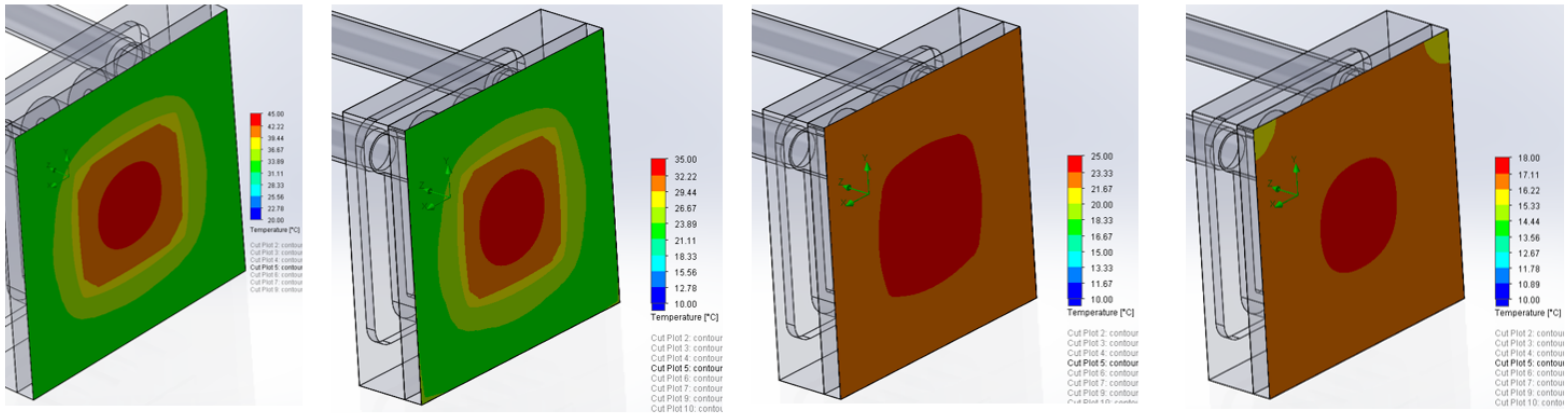

Fig. 14 Temperature distribution on the outer surface of the chip carrier

Case	A	B	C	D
Distance:	1 cm	1 cm	1 cm	1cm
Heat generation rate:	30 W	30 W	30 W	30 W
- To Photovoltaic Cell:	12.3 W	12.3 W	12.3 W	12.3 W
- To Chip Carrier:	12.3 W	12.3 W	12.3 W	0 W
H2O Temp:	20 C	10 C	10 C	10 C
Chip Carrier Material:	316 Stainless Steel	316 Stainless Steel	Copper	Copper

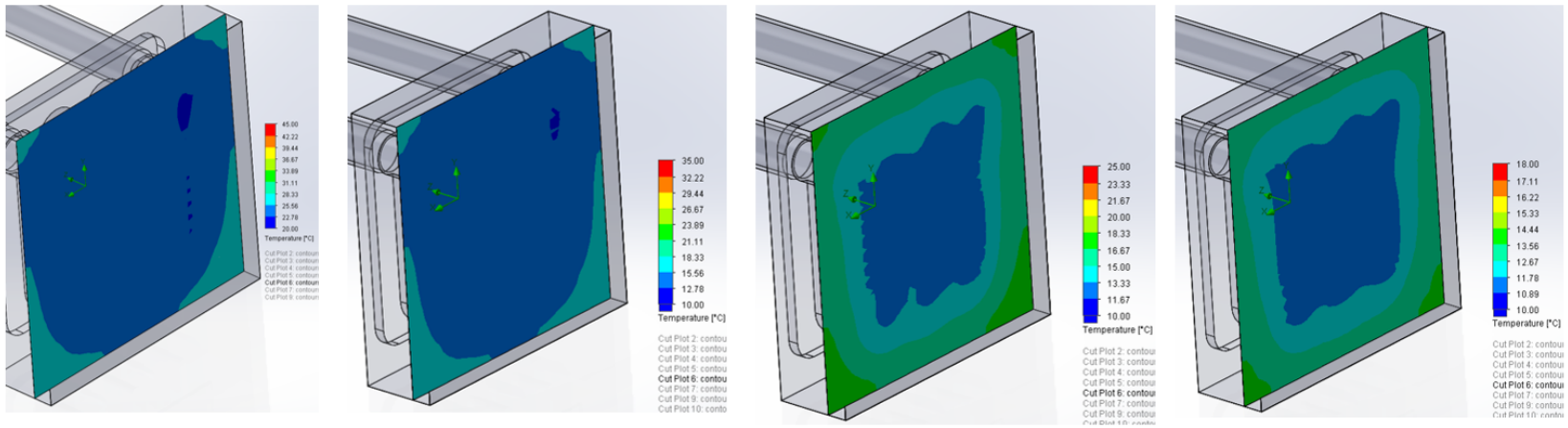

Fig. 15 Temperature distribution where the chip carrier contacts the heat sink

Case	A	B	C	D
Distance:	1 cm	1 cm	1 cm	1cm
Heat generation rate:	30 W	30 W	30 W	30 W
- To Photovoltaic Cell:	12.3 W	12.3 W	12.3 W	12.3 W
- To Chip Carrier:	12.3 W	12.3 W	12.3 W	0 W
H2O Temp:	20 C	10 C	10 C	10 C
Chip Carrier Material:	316 Stainless Steel	316 Stainless Steel	Copper	Copper

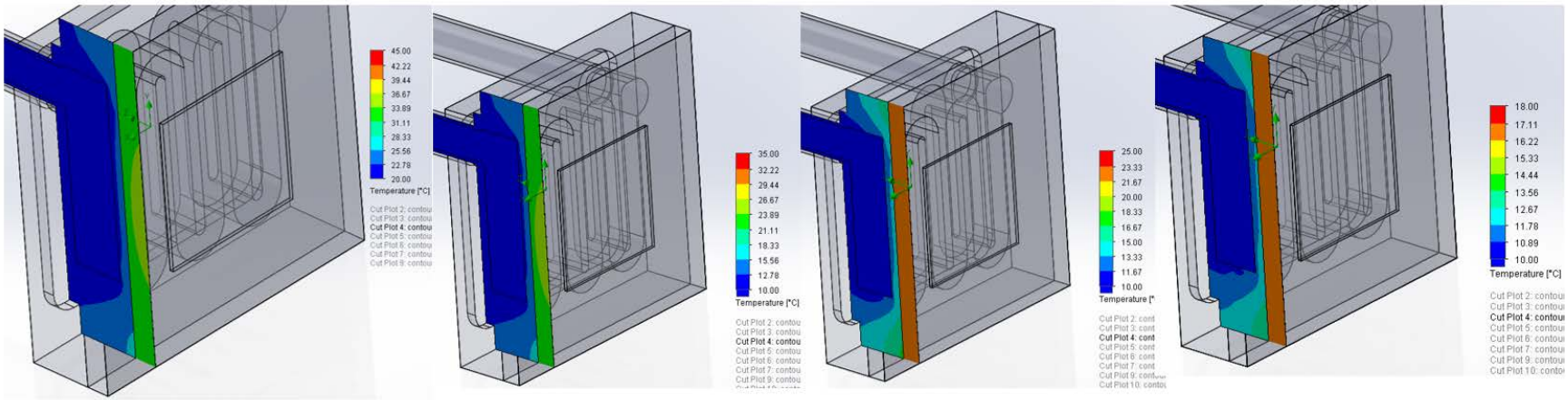

Fig. 16 Temperature distribution through the center line of the outlet tube and through a portion of the heat sink and chip carrier

Figure 12 shows the temperature profile for a cross section through the center of the assembly. As expected, the photovoltaic cell was the hottest component and the cooling water the coldest. The temperature of the photovoltaic cell was 45 °C for Case A, 35 °C for Case B, 25 °C for Case C, and 18 °C for Case D. In all cases, the cooling water was minimally affected by the different conditions, indicating that the cooling water and the serpentine flow path were adequate for the application. To lower the temperature of the photovoltaic cells, the cooling water temperature was lowered. Comparing Case A and B, lowering the water temperature from 20 to 10 °C, lowered the temperature of the photovoltaic cell by 10 °C. To enable room-temperature operation, the chip carrier material was changed from 316 stainless steel to copper, resulting in better heat spreading and conduction to the heat sink. With all the parameters the same except the chip carrier material, Case C with the copper chip carrier had a photovoltaic temperature of 25 °C compared to 35 °C for Case B. Note the temperature range of the 316 stainless steel chip carrier in Case B was greater than the copper version shown in Case C even though all other conditions were the same. This was the result of the tremendous difference in the thermal conductivity of copper compared to 316 stainless steel. Cases A and B show a temperature difference between the water and the photovoltaic cell at 25 °C. In comparison with the copper chip carrier, Case C had a difference is 15 °C and Case D a difference of 8 °C.

Figure 13 shows the temperature distribution on the outer surface of the photovoltaic cell. Cases A and B show a 9 °C temperature range, while the Case C and D temperature range is 2 °C. Cases C and D have a more even temperature distribution due to the greater effectiveness of the copper chip carrier to transfer heat compared to Cases A and B with the 316 stainless steel version.

Figure 14 shows the temperature distribution on the outer surface of the chip carrier. Cases A and B show a temperature range 14 °C, while Case C shows a 4 °C range and Case D a 3 °C range. Note again Cases C and D show a more even temperature profile due to the greater effectiveness of the copper chip carrier to transfer heat compared to Cases A and B with the 316 stainless steel version.

Figure 15 shows the temperature distribution where the chip carrier contacts the heat sink. Cases A and B show a temperature range of 8 °C, while Case C has a 6 °C range and Case D a 4 °C range. The range of temperatures for this cross section for the 4 cases is more similar due to the closer proximity to the cooling water.

Figure 16 shows the temperature distribution through the center line of the outlet tube and through a portion of the heat sink and chip carrier. The difference between the water temperature and the heat sink is 8 °C in Cases A and B, 6 °C in Case C, and 3 °C in Case D. This shows the copper is helping transfer the heat to the heat

sink. Since the heat sink temperature nearly matches the cooling water temperature, the heat sink appears adequate for the application. Note the large change in temperature at the interfaces between the heat sink and the chip carrier. This is caused by the thermal contact resistance.

Figures 17 and 18 show the results of cases where the power from the emitter was 70 W and the distance from the emitter to the chip carrier was either 1 mm or 1 cm. For the case where the distance is 1 mm, this results in the application of 63.6 W to the surface of the photovoltaic cell and 6.3 W to the surface of the chip carrier not covered by the photovoltaic cell. For the case where the distance is 1 cm, this results in the application of 28.7 W to both the surface of the photovoltaic cell and the surface of the chip carrier not covered by the photovoltaic cell. In both cases, the chip carrier is 316 stainless steel and the cooling water temperature is 10 °C.

Case	E	F
Distance:	1 mm	1 cm
Heat generation rate:	70 W	70 W
- To Photovoltaic Cell:	63.6 W	28.7 W
- To Chip Carrier:	6.3 W	28.7 W
H2O Temp:	10 C	10 C
Chip Carrier Material:	316 Stainless Steel	316 Stainless Steel

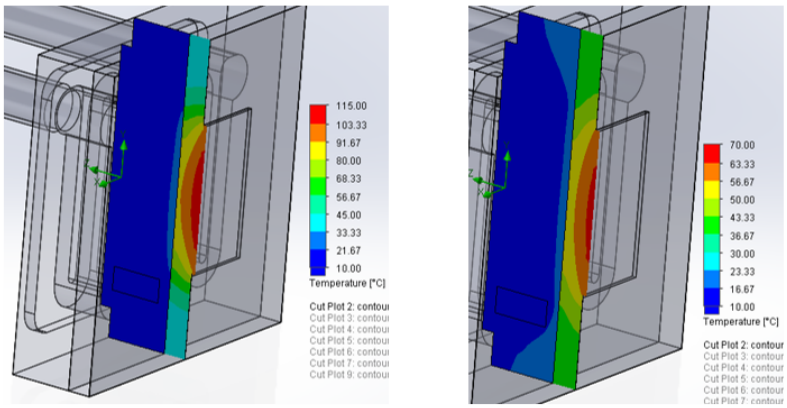

Fig. 17 Temperature distribution for a cross section through the center of the assembly

Case	E	F
Distance:	1 mm	1 cm
Heat generation rate:	70 W	70 W
- To Photovoltaic Cell:	63.6 W	28.7 W
- To Chip Carrier:	6.3 W	28.7 W
H2O Temp:	10 C	10 C
Chip Carrier Material:	316 Stainless Steel	316 Stainless Steel

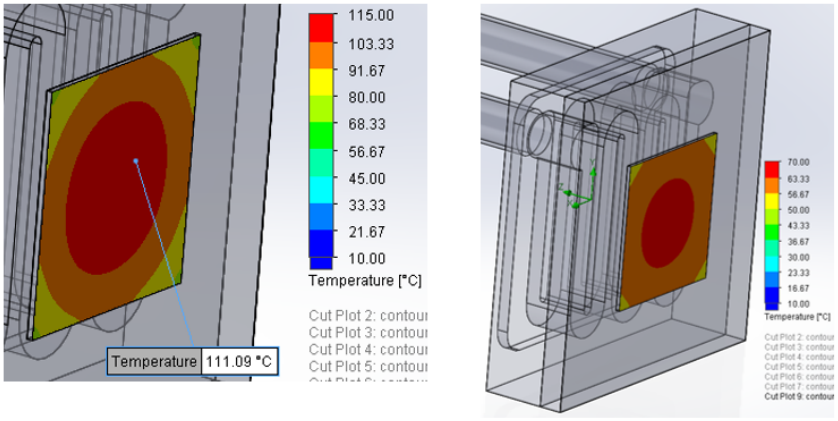

Fig. 18 Temperature distribution on the outer surface of the photovoltaic cell

Figure 17 shows the temperature distribution for a cross section through the center of the assembly. Figure 17 shows Case E where the distance between the chip carrier and the emitter is 1 mm, the photovoltaic temperature reaches 115 °C, whereas in Case F where the distance is 1 cm, the temperature is 70 °C. In Case E, the heat sink temperature rise is of up to 33 °C in the area shadowed by the photovoltaic cell. In Case F where the emitter is 1 cm away and more power is applied to the surface of the chip carrier not covered by the photovoltaic cell, the heat sink temperature rises up to 13 °C and further into the heat sink at the outer edges than in the area shadowed by the photovoltaic cell. In Case E, the outer edges of the chip carrier reached 45 °C, while in Case F the outer edge reached 36 °C. There may be some room for improvement in this area by changing the heat sink material to copper. Note the chip carrier in both of these cases was 316 stainless steel. Future analysis should include cases with copper chip carriers.

Figure 18 shows the temperature distribution on the outer surface of the photovoltaic cell. Case E shows a temperature range from 68 to 115 °C, while Case F ranges from 50 to 70 °C. It is anticipated the performance of the photovoltaic cells will be reduced compared to operation at room temperature. It is anticipated that having a copper chip carrier in these cases might reduce the temperature distribution. See the Appendix for figures showing the other cross section views for Cases E and F.

6. Conclusion

To support the development of the TPV concept demonstrator, a water-cooled heat sink is needed to control the temperature of the photovoltaic cells while exposed to the radiation from the emitter. The heat sink design goal is to control the temperature of the photovoltaic cells to at least as low as room temperature (25 °C). Controlling the temperature of the photovoltaic cells will allow for a parametric study of the effect of temperature on photovoltaic cell performance.

This report shows the analysis of a heat sink and chip carrier design to meet this design goal. Assuming 30 W is emitted by the emitter on one side of the combustor with a distance between the emitter and the photovoltaic cell of 1 cm, the analysis shows the design heat sink with the copper chip carrier and 10 °C cooling water will control the photovoltaic temperature to 25 °C. These conditions are being incorporated into the demonstration system heat sink and chip carrier design. The temperature of the underside of the photovoltaic cell will be monitored during testing to see how well the analysis compares to reality.

7. Future Studies

Comparing the data collected during testing with that predicted by the analysis is key to planning future studies. If the current design is unable to control the temperature of the photovoltaic cells, more work will need to be done to improve the analysis, especially since the emitter will be closer to the photovoltaic cell in future tests. As identified earlier, one key parameter is the thermal contact resistance. Using the data collected during testing, this parameter could be modified to fit reality. Ideally, additional thermocouples could be added to measure the temperature at other points to adjust the parameters.

8. References

1. Waits MC. Thermophotovoltaic energy conversion for personal power sources. Adelphi (MD): US Army Research Laboratory (US); 2012 Feb. Report No.: ARL-TR-5942.

2. Thermal fluid analysis. Waltham (MA): Solid Works; 2015 [accessed 2015]. http://www.solidworks.com/sw/products/simulation/thermal-fluid-analysis.htm.

3. Incropera FP, DeWitt DP. Fundamentals of heat and mass transfer. 2nd ed. New York (NY): John Wiley & Sons; 1985. p. 68.

4. Chubb DL. Fundamentals of thermophotovoltaic energy conversion. Amsterdam (Netherlands): Elsevier; 2007.

INTENTIONALLY LEFT BLANK.

Appendix. Cases E and F

Case	E	F
Distance:	1 mm	1 cm
Heat generation rate:	70 W	70 W
- To Photovoltaic Cell:	63.6 W	28.7 W
- To Chip Carrier:	6.3 W	28.7 W
H2O Temp:	10 C	10 C
Chip Carrier Material:	316 Stainless Steel	316 Stainless Steel

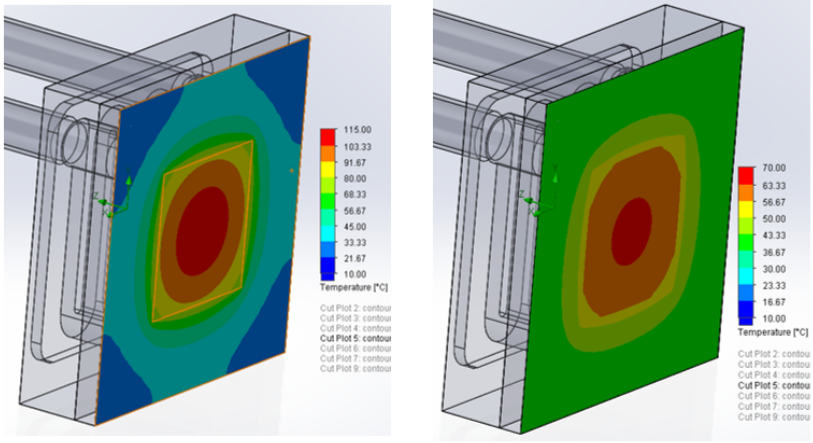

Fig. A-1 Case E

Case	E	F
Distance:	1 mm	1 cm
Heat generation rate:	70 W	70 W
- To Photovoltaic Cell:	63.6 W	28.7 W
- To Chip Carrier:	6.3 W	28.7 W
H2O Temp:	10 C	10 C
Chip Carrier Material:	316 Stainless Steel	316 Stainless Steel

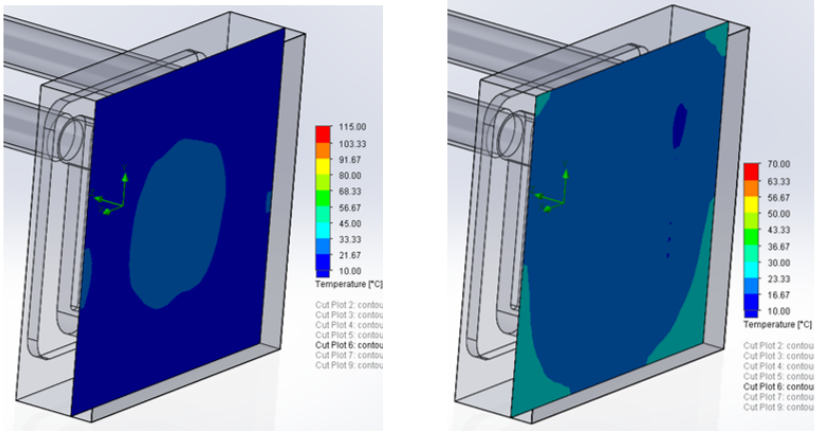

Fig. A-2 Case F

1 (PDF) DEFENSE TECHNICAL INFORMATION CTR DTIC OCA

2 (PDF) DIRECTOR US ARMY RESEARCH LAB RDRL CIO L IMAL HRA MAIL & RECORDS MGMT

1 (PDF) GOVT PRINTG OFC A MALHOTRA

2 (PDF) DIRECTOR US ARMY RESEARCH LAB RDRL SED E WR ALLMON CM WAITS

INTENTIONALLY LEFT BLANK.